A robust Automated Scan Prescription in MRI liver scans

Takao Goto[1], and Hiroyuki Kabasawa[1]
[1]*Global Applied Science Laboratory, GE Healthcare, Hino-shi, Tokyo, Japan*

Introduction

Automated scan prescription is a valuable tool for not only simplifying the workflow, but also achieving accurate and consistent slice positioning in an operator-independent environment. In our previous studies [1], we have demonstrated successful automated prescriptions for MRI liver scans using the Active Shape Model (ASM)[2]. Practically speaking, however, the liver shape of the patient frequently differs from the established normal liver shape either due to the incidence of disease (HC or HCC) or as a side effect of surgery. In this study, we propose a new automated scan prescription algorithm for the various shape of livers. Test results from normal volunteers and simulated deformed livers demonstrate the efficacy of the proposed approach.

Methods

The planning stage of a MR liver scan primarily involves the determination of the axial planes between the superior and inferior margins of the liver via the identification of these edges on the localized image. The accurate detection of both edges is an important requirement regardless of the shape of the liver. Figure 1 illustrates the block diagram of our proposed method. The 3D scout volume data (256x256x120) was acquired using the same protocol defined in our previous study, which employed the T1-weighted Fast SPGR sequence (LAVA-XV) with breath holding. In the pre-processing step, a 3D- median filter and noise level detection were applied successively to the scout data to achieve noise reduction and thresholding. This subsequently helped to identify the desired body area in the 2D-projection images. In the next step, a limited number of slices were used to produce 2D-projection images to prevent edge blurring. Subsequently, the upper edge of the liver was located by determining the maximum cross-correlation with the profile template, which is the sum of several rows in the coronal projection image. A small ROI selected by scaling down the mean shape of the liver is identified on the liver based on the anchor point in order to collect statistical information on the liver (Figure 2). The S/I location of the ROI is the same as the upper edge of the liver. The R/L location is the peak of the average signal inside the ROI, when the ROI traverses the image from the right to the left edge. The pixel data inside the ROI was used to calculate the mean (μ_l) and variance (σ_l^2) of the pixel, as well as the mean (μ_n) and variance (σ_n^2) of the eight neighboring pixels. The Gibbs distribution was adopted as a prior probability using the μ_n and the σ_n to distinguish the lower liver edge from the surrounding organs and tissues that have intensity similar to that of the liver; such obstacles are more inhomogeneous than the liver. In contrast, the signal distribution of the liver was expressed by the Gauss distribution using μ_l and σ_l. The posterior probability was obtained from both the Gibbs and Gauss distributions using Bayes' theorem. A small region containing 5x5 pixels was selected to apply the MAP estimate using posterior probability, resulting in a combination of a likelihood function and the prior probability. A higher posterior probability indicates that such a region has a higher possibility of belonging to the liver. The highest peak is located at the liver edge when the two regions that are located on either side (top and bottom) of the point of interest are subtracted. The lower edges can be located without any shape constraint (such as in the ASM) by moving two such regions to the bottom of every row in the image. This demonstrates the efficacy of our method on deformed livers. Following institutional review and approval, our method was tested on 45 healthy volunteers. In addition, deformed livers were simulated based on clinical information and 12 such datasets were tested offline using our proposed method.

Results and Discussion

Table 1 shows the edge detection error in the volunteer and simulated data, which was calculated by subtracting the manually identified edge and that determined by the proposed algorithm in the 3D volume images. Since there is a clear boundary between the lung and the liver, the standard deviation of the positioning error at the upper edge was much less than that at the lower edge. However, this is acceptable as 7-8 mm thickness and 1-2 mm spacing are commonly employed as the parameters for the axial planes and two missing slices are equivalent to 14-20 mm. Figure 3 shows the results from applying the proposed algorithm to the simulated livers in the 2D coronal projection image. In Figure 3 (a), the deformed liver has a larger left lobe as compared to the right. Such a deformation is representative of a patient liver post-surgery. On the other hand, in Figure 3 (b), the deformed liver has a larger right lobe, indicating liver enlargement. The dotted line shows the detected lower edge. When compared to the results produced by the ASM (white line), the proposed method detected the lower edge accurately, while the ASM could not due to the shape constraint imposed by a normal liver. The computation time was approximately 10 seconds on a Core i5 laptop with a 2 GB memory.

Conclusion

We proposed a new method for automated scan prescription in MRI liver imaging, and demonstrated the efficacy of our algorithm for deformed livers within practical computation time constraints. The application of the MAP estimate combined with statistical information from the ROI enabled the detection of liver edges of various shapes, thus, signifying a good clinical technique. Future work will include modifications to vary the MAP estimate region size iteratively in order to achieve higher accuracy.

Reference

1. T. Goto and H. Kabasawa, ISMRM2011 4533
2. T. F. Cootes et al., Imag and Vision Comp 12: 355-366 (1994)

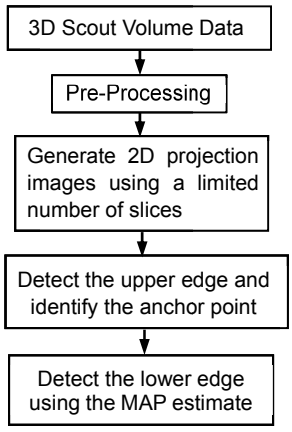

Figure 1 Block diagram

Error [mm]	Mean	S.D.	Max.
Upper Edge	1.87	2.04	6.0
Lower Edge	-0.9	7.84	21.0

Table 1 Detection error of lower and upper edges

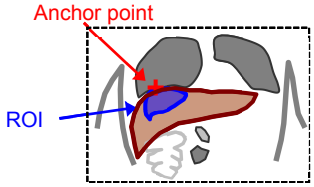

Figure 2 ROI placement based on the anchor point

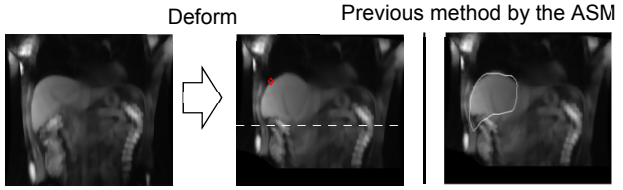

(a) Simulating a larger left lobe and smaller right lobe

(b) Simulating a larger right lobe

Figure 3 Detection results for the simulated deformed liver